Journal of Power Sources 193 (2009) 233–240

Contents lists available at ScienceDirect

Journal of Power Sources

journal homepage: www.elsevier.com/locate/jpowsour

Thermodynamic model for an alkaline fuel cell

Ivan Verhaert[a,b,c,*], Michel De Paepe[a], Grietus Mulder[c]

[a] Department of Flow, Heat and Combustion Mechanics, Ghent University - UGent, Sint-Pietersnieuwstraat 41, 9000 Gent, Belgium
[b] KHKempen, University College, Kleinhoefstraat 4, 2440 Geel, Belgium
[c] VITO, Flemish Institute for Technological Research, Boeretang 200, 2400 Mol, Belgium

ARTICLE INFO

Article history:
Received 9 October 2008
Received in revised form 13 February 2009
Accepted 16 February 2009
Available online 25 March 2009

Keywords:
Alkaline fuel cell
Model
Heat management
Cogeneration
Performance

ABSTRACT

Alkaline fuel cells are low temperature fuel cells for which stationary applications, e.g. cogeneration in buildings, are a promising market. In order to guarantee a long life, water and thermal management has to be done in a careful way. In order to better understand the water, alkali and thermal flows, a two-dimensional model for an Alkaline Fuel Cell is developed using a control volume approach. In each volume the electrochemical reactions together with the mass and energy balance are solved. The model is created in Aspen Custom Modeller, the development environment of Aspen Plus, where special attention is given to the physical flow of hydrogen, water and air in the system. In this way the developed component, the AFC-cell, can be built into stack configurations to understand its effect on the overall performance. The model is validated by experimental data from measured performance by VITO with their Cell Voltage Monitor at a test case, where the AFC-unit is used as a cogeneration unit.

1. Introduction

Fuel cell technology permits to generate emission-free electricity, using hydrogen as fuel and producing water and heat instead of polluting exhaust gases. The alkaline fuel cell (AFC) was the first to be put in practical service in space applications. However, despite of its early success the current research and development activities are more directed towards proton exchange membrane fuel cells (PEMFC) as the technology of choice for vehicular applications [1]. Also more research is devoted to high temperature fuel cells as the solid oxide fuel cell (SOFC) and molten carbonate fuel cell (MCFC) which show some interesting prospectives in new power cycles for electricity plants [2–4]. In a changing climate of energy supply and demand, smart grids with distributed generation as, e.g. micro-cogeneration can be the future for our energy market [5]. Compared to other micro-cogeneration technology fuel cells show the highest electrical efficiency, and are promising systems for residential and small-scale cogeneration applications [6]. The main reason for its high performance is its modular construction: therefore its efficiency is hardly influenced by its size. [7] In spite of the limited development efforts for AFC technology it is still competitive with other fuel cells for power applications. Further improvement in the AFC technology is still possible and will strengthen this position [1]. Intensys[1] has developed an AFC-system which can be used as a cogeneration unit. With help from the VITO the system is CE approved and commercially available. [8] The system is operational in Vilvoorde and Hasselt as a demonstration project. Experimental data is generated to examine its performance in time and at different operation modes. Advancements, regarding overall thermodynamic behaviour and overall efficiency, are still possible. In this work a model of an alkaline fuel cell is built in Aspen Custom Modeller. This model focuses on the thermal management of the AFC with circulating electrolyte. With this model several system designs can be examined in Aspen Plus, in order to initiate further improvement.

2. Thermodynamics of an alkaline fuel cell

2.1. General operation

An AFC operates by introducing hydrogen at the anode and oxygen/air at the cathode.

- At the hydrogen inlet a gas mixture of water vapour and hydrogen enters the gas chamber of the fuel cell. The hydrogen diffuses out of the gas chamber into the working area of the anode.
- At the oxygen inlet CO_2-free air or pure oxygen arrives in the gas chamber. The oxygen diffuses into the working area of the cathode to take part in the reaction.

Both electrodes, anode and cathode, are separated by a circulating electrolyte, a 6 M potassium hydroxide solution (Fig. 1). At the anode hydrogen reacts with hydroxyl ions into water and free

* Corresponding author at: KHKempen, University College, Kleinhoefstraat 4, 2440 Geel, Belgium. Tel.: +32 473 53 92 25; fax: +32 14 58 48 59.
E-mail address: ivan.verhaert@khk.be (I. Verhaert).

[1] Intensys BVBA, Hoge Mauw, Arendonk, Belgium, http://www.intensys.com.

0378-7753/$ – see front matter © 2009 Elsevier B.V. All rights reserved.
doi:10.1016/j.jpowsour.2009.02.095

Nomenclature

hA	overall conductance ($W K^{-1}$)
A	effective area of the fuel cell (m^2)
E_{Nernst}	thermodynamic potential (V)
F	Faraday's constant ($C mol^{-1}$)
G	Gibbs free energy ($J kg^{-1}$)
h	total enthalpy ($J kg^{-1}$)
I	load current (A)
m	mass flow rate of species i ($kg s^{-1}$)
Mi	molecular weight of species i ($kg mol^{-1}$)
pi	(partial) pressure (bar)
P	power (W)
Q	heat (W)
R	universal gas constant ($J mol^{-1} K^{-1}$)
T	temperature (°C)
U	voltage (V)
v	velocity
Re	Reynolds number
Nu	Nusselt number
c_i	coefficient for the electrochemical model

Greek symbols

α	transfers coefficient
η	overvoltage (V)

Subscripts

an	anode
cat	cathode
FCB	fuel cell body
e	electrical
el	electrolyte
surr	surroundings
w	water/water vapour

electrons (Eq. (1)).

$$H_2 + 2(OH)^- \rightarrow 2H_2O + 2e^- \quad (1)$$

Within the electrolyte, the water is transported from the anode to the cathode. An external electric circuit leads the electrons to the cathode. At the cathode oxygen reacts with water and electrons in hydroxyl ions (Eq. (2))

$$H_2O + \tfrac{1}{2}O_2 + 2e^- \rightarrow 2(OH)^- \quad (2)$$

These ions flow from cathode to anode through the electrolyte, to sustain the total electrochemical reaction. Combining both reactions the overall reaction (Eq. (3)) shows that the end product is water, which can be removed in one or both gas streams or in the electrolyte, depending on the fuel cell configuration.

$$H_2 + \tfrac{1}{2}O_2 + 2e^- \rightarrow H_2O \quad (3)$$

The overall reaction is exo-energetic. This energy has an electric part, which is consumed in the external electric circuit, and a thermal part, which results in a temperature rise inside the fuel cell. To maintain the overall fuel cell temperature, heat is removed by outlet mass flows or by losses to the environment.

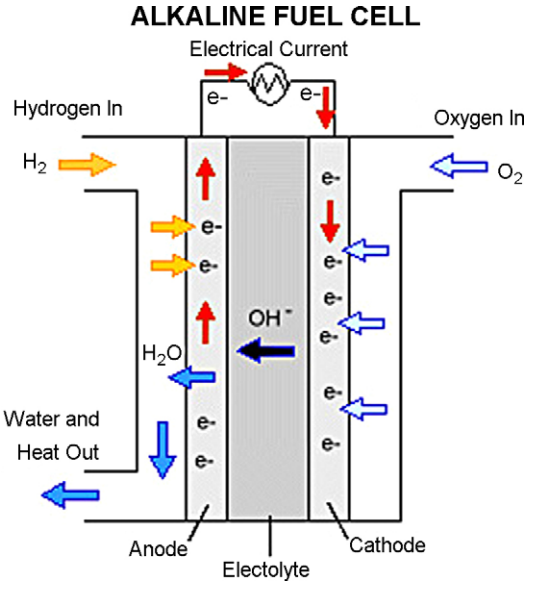

Fig. 1. Working Principle of an Alkaline Fuel Cell (source: *U.S. Dept. of Energy-EERE*).

2.2. Overview of AFC models

To predict fuel cell performance in order to improve it, mathematical models were developed to predict electrical power. In the early nineties Kimble and White proposed a model for a complete fuel cell, where they take into account the polarization and physical phenomena going on in the solid, liquid and gaseous phase of both anode, separator and cathode regions, assuming a macro homogeneous, three-phase porous electrode structure [9]. The model divides the fuel cell in five layers, a gas diffusion layer and reaction layer for both anode and cathode and a separator, containing the electrolyte. In 1999 this model was the basis for the model of Jo and Yi, where they corrected some invalid correlations and parameters, e.g. in the open-circuit potential and the liquid diffusion parameters [10]. Both Kimble and White and Jo and Yi used immobilized or re-circulating electrolyte and removed water in the gas streams. In 2006 Duerr et al. translated the model of Jo and Yi to a stack-model in a Matlab/Simulink environment and added dynamics to the electrical part of the model [11]. Few details were given on the calculation method and the estimation method of some physical parameters. These models are all meant to predict the polarization curve or electric response of the fuel cell. In 1998 Rowshanzamir et al. studied the mass balance and water management in the AFC [12] by only applying mass balances and diffusion laws (Stefan-Maxwell) for the gas diffusion layer. However their model does not provide any prediction on fuel cell performance. Because of the fuel cell type, each model could make an assumption on water disposal. All stipulated that water was removed in both gas streams or (for the Orbiter) in the hydrogen stream. The fuel cell (system) which is subject of our research removed water by both exhaust gases and electrolyte flow. After the fuel cell, all these streams are collected in one reservoir, where eventually at nominal working point, the air flow is responsible for the disposal of water (vapour).

2.3. Model development

Using the same methodology of H. Huisseune et al. [13] for PEMFC a 1D/2D-model with control volume approach is obtained with following assumptions.

- Dynamic pressure losses within the fuel cell are neglected. In this way the total pressure can be assumed constant over the entire fuel cell.
- The temperature is assumed to be uniform in each control volume and all output flows have this temperature.
- The partial pressures within the control volume are the mean of the input and output flow in the second dimension.
- The heat losses from the gas chambers to the environment are neglected, because the heat exchanging surface is relatively small.

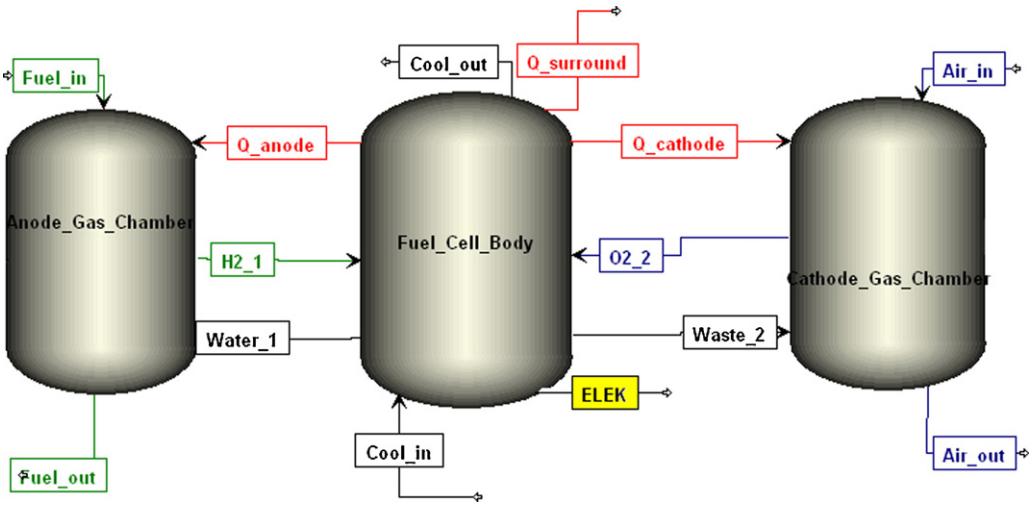

Fig. 2. Model of the alkaline fuel cell (in Aspen Custom Modeller).

All heat losses to the environment are therefore modelled as heat losses of the fuel cell body to the environment.

The three parts which were considered in the control volume model, are the anode and cathode gas chambers and the fuel cell body, where the reaction takes place (Fig. 2). The model is modularly built. In this way a more detailed model can be obtained by serially connecting several individual models. Fig. 2 shows a screen shot of an individual model in Aspen Custom Modeller.

For each control volume a mass and energy balance is used. The energy balances are closed by heat fluxes which are exchanged between neighbouring control volumes or between a control volume and the environment. This heat flux is modelled as a convective heat flux. Next to heat and mass transfer between control volumes, also electric energy, generated in the fuel cell body is transferred to the environment. For every control volume the mass and energy balances are specified. Next an electrochemical model is used to describe the electric behaviour of the fuel cell.

2.3.1. Anode gas chamber

Mass balance:

The fuel, a mixture of hydrogen and water vapour, enters the gas chamber, where the hydrogen diffuses to the fuel cell body to react. A part of the water, formed during the reaction, diffuses as water vapour back into the hydrogen gas chamber. A mixture of unused fuel and water vapour leaves the gas chamber to a next stage.

$$\begin{aligned} &m_{\mathrm{H_2},Fuel-in,an} - m_{\mathrm{H_2},Fuel-out,an} = m_{\mathrm{H_2},Hydrogen} \\ &m_{w,Fuel-out,an} - m_{w,Fuel-in,an} = m_{w,vapour} \end{aligned} \quad (4)$$

Energy balance:

$$\begin{aligned} &\Sigma_i m_{i,in,an} \cdot h_{i,in,an} - \Sigma_i m_{i,out,an} \cdot h_{i,out,an} = Q_{an} \\ &-Q_{FCB,an} = Q_{an} \\ &Q_{FCB,an} = hA_{FC,an}.(T_{FCB} - T_{an}) \end{aligned} \quad (5)$$

As boundary condition in the simulation the fuel entering the (first) gas chamber is pure hydrogen and there is no hydrogen leaving the (last) gas chamber as unused fuel, because it is an end-of-pipe system.

2.3.2. Cathode gas chamber

Mass balance:

The entering air contains oxygen, nitrogen and water vapour. There is a large excess of air because air is used to remove water vapour from the cathode. While oxygen diffuses to the fuel cell body, water vapour diffuses into the gas stream.

$$\begin{aligned} &m_{\mathrm{O_2},Fuel-in,cat} = m_{\mathrm{O_2},Oxygen} + m_{\mathrm{O_2},Fuel-out,cat} \\ &m_{w,Fuel-in,cat} + m_{w,vapour} = m_{w,Fuel-out,cat} \\ &m_{\mathrm{N_2},Fuel-in,cat} = m_{\mathrm{N_2},Fuel-out,cat} \end{aligned} \quad (6)$$

Energy balance:

$$\begin{aligned} &\Sigma_i m_{i,in,cat} \cdot h_{i,in,cat} + Q_{cat} = \Sigma_i m_{i,out,cat} \cdot h_{i,out,cat} \\ &Q_{cat} = Q_{FCB,cat} \\ &Q_{FCB,cat} = hA_{FC,cat}.(T_{FCB} - T_{cat}) \end{aligned} \quad (7)$$

The cathode outlet temperature is one of the main parameters on which the model is validated.

2.3.3. Fuel cell body

Mass balance:

Within the fuel cell body, the driving electrochemical reaction takes place. The mass and molar balance relates the hydrogen and oxygen consumption to the generation of water and electric current. The current is linked to the molar flows by Faraday's law.

$$\begin{aligned} &m_{w,el-in,FCB} + \frac{M_w \cdot I_{cell}}{2F} = \\ &m_{w,el-out,FCB} + m_{w,cat} + mw, an \\ &m_{\mathrm{H_2},Hydrogen} = \frac{M_w \cdot I_{cell}}{2F} \\ &m_{\mathrm{O_2},Oxygen} = \frac{M_w \cdot I_{cell}}{4F} \end{aligned} \quad (8)$$

Energy balance:

Within the fuel cell body the different layers, gas diffusion, catalytic and separator layer are enclosed [9–11]. Although different layers exist in the fuel cell, in this paper the properties of the electrolyte/separator are taken to define the thermodynamic behaviour of the fuel cell body. The mass flows between fuel cell body and gas chamber however will only consist of gas in accordance to the boundary conditions of the gas diffusion layers. This will affect the enthalpy of these stream and will limit the mass flow, because the

partial pressure cannot exceed the saturation pressure.

$$\Sigma_i m_{i,in,FCB} \cdot h_{i,in,FCB} = \Sigma_i m_{i,out,FCB} \cdot h_{i,out,FCB} + Q_{FCB} + P_e$$
$$Q_{FCB} = Q_{FCB,sur} + Q_{FCB,cat} + Q_{FCB,an}$$
$$Q_{FCB,sur} = hA_{FCB,sur}.(T_{FCB} - T_{sur*}) \quad (9)$$

The energy balance of the fuel cell body consists not only of incoming and outgoing mass streams (with certain enthalpy) and heat flows, but also of an electric power output. This output is more detailed in the electrochemical model.

2.3.4. Electrochemical model

The goal of the presented research is to find a model which can predict outlet temperatures, next to electrical output. Therefore the electrochemical model is based on a parameter approach of the polarization curve, which relates current to voltage and operating parameters and is able to show effects of composition, flow rate, temperature,. . . on the cell performance [14]. The electric power is a product of both current and voltage. Current can be determined using Faraday's law. The fuel cell voltage is defined by the Nernst potential, the activation overvoltage, the ohmic voltage and the diffusion losses.

$$P_e = U \cdot I \quad (10)$$

$$U = E_{Nernst} - \eta_{act} - \eta_{res} - \eta_{diff} \quad (11)$$

The Nernst potential is calculated out of the Gibbs free energy from the electrochemical reaction. Gibbs free energy is calculated using the properties and libraries of Aspen environment.

$$E_{Nernst} = -\frac{\Delta G_0}{2F} + \frac{RT_{cell}}{2F}\left[ln(p_{H_2}) + \frac{1}{2}ln(p_{O_2})\right] \quad (12)$$

The activation, ohmic and diffusion losses are calculated by the equations found in literature [15,16]. To calculate these losses following expressions ((13), (14) and (15)) are used.

$$\eta_{act} = \frac{R \cdot T}{\alpha \cdot n \cdot F} ln\left(\frac{I_{cell}/A}{j_0}\right) \quad (13)$$

$$\eta_{res} = R_e \cdot I_{cell} \quad (14)$$

Table 1
List of the used semi-empiric parameters.

Parameter	Value	Improved Model
j_L	2000 A m^{-2}	2000 A m^{-2}
α	0.1668	0.1668
c_1	174, 512 (A m^{-2})	174, 512 (A m^{-2})
c_2	5485 (K)	5485 (K)
c_3	0.0045 Ω	0.0045 Ω
c_4	5.9e − 5 Ω K^{-1}	5.9e − 5 Ω K^{-1}
hA_{an}	3.2 W K^{-1}	
hA_{cat}	6.4 W K^{-1}	
c_5		2.016e − 4
c_6		1.5
hA_{sur}	51.2 W K^{-1}	51.2 W K^{-1}

$$\eta_{diff} = \frac{R \cdot T}{\alpha \cdot n \cdot F} ln\left(\frac{j_L}{j_L - I_{cell}/A}\right) \quad (15)$$

The activation overvoltage, given by Eq. (13), is a function of the exchange current, j_0, which is temperature dependent given by Eq. (16).

$$j_0 = c_1 \cdot exp\left(\frac{-c_2}{T_{cell}}\right) \quad (16)$$

The ohmic resistance is a result of resistance due to resistance of electron collector and a term inversely related to conductivity of the electrolyte. This conductivity is related to the cell temperature. This relation results in a linear expression (Eq. (17))

$$R_e = c_3 - c_4 \cdot T_{cell} \quad (17)$$

2.3.5. Discussion on parameter estimation

The empiric model shows great similarity to the one used by Amphlett et al. [17] and later by Huisseune et al. [13] for their modelling on PEM fuel cells. The general equations are useful for all types of fuel cells. The parameters however will differ. All physical properties (enthalpy, Gibbs free energy,. . .) are linked to the libraries of the Aspen environment. A number of parameters however are semi-empiricly obtained. Table 1 shows all the semi-empiric parameters for this model. In this paragraph a brief discussion on every parameter is included.

At a certain current density, j_L, the diffusion losses will be too high. The value is based on stack construction (See Section 3.1), maximum current and active cell area ($A = 0.064\,m^2$). Ref. [16]

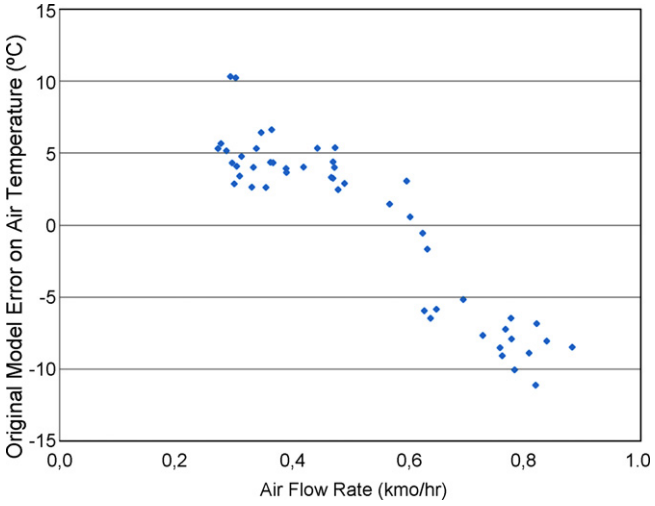

Fig. 3. Experimental set-up.

shows for other fuel cell types values of $20,000\,A\,m^{-2}$. The relatively low value is due to the use of air instead of oxygen (reduction by a factor 5) and due to the low development rate in AFC technology. The activation parameters are a best fit for the measured data, within an acceptable range. Those ranges went for α from 0.1 to 0.5 and for j_0 from $10^{-4}\,A\,cm^{-2}$ or $1\,A\,m^{-2}$ to $10^{-9}\,A\,cm^{-2}$ or $10^{-5}\,A\,m^{-2}$. The resistive parameters are in the same order as those in [17,13] for PEMFC. For the convective values we can refer again to Amphlett et al. [17] and Huisseune et al. [13]. Similar results are shown for a stack of the same size. Both anode and cathode transfer coefficient are in a similar range. The transfer coefficient to the surroundings is higher because here the system consists out of 4 stacks and in [17,13] only one stack is considered which is more compact. In a first model approach the convective heat transfer coefficient was fixed, although it is function of amongst others, temperature and velocity. Especially this last influence parameter seemed inneglectible. In the model validation it is shown that at high air flow rates (overflow) the model underestimates the air temperature. Therefore both convection coefficients are configured as a function of the gas flow rate (Eq. (18)). This resulted in much better experimental validation (See Section 4).

$$hA_{cat} = hA_{an} = c_5 \cdot v^{c_6} \tag{18}$$

3. Experimental work

3.1. Experimental set-up

Experimental tests for model validation were done at the VITO on the AFC-system of the KHLim. Fig. 3 shows a schematic view of the experimental set-up [8]. The system consists of 4 stacks. The stacks are supplied with ambient air at a measured temperature (measuring point a). The air flow is regulated by an electric fan with variable speed. The air flow rate is indirectly measured by the electric current absorbed by the fan motor (point b). Earlier measurements show a linear correlation between this current and the air flow rate in the nominal working range. The air is guided through a CO_2-scrubber, where a slight temperature rise is expected (point c is estimated). The air is parallel divided over the stacks. Within every stack the air is again parallel divided over the different cells. The air overflow will be guided to the electrolyte tank, but because other configurations will be examined this is not yet incorporated in the drawing. The outlet air temperature is measured (point d). A centrifugal pump pumps the electrolyte (point e) out of an electrolyte reservoir and enables the circulation of the electrolyte. The electrolyte flow is indirectly measured (point e) in the same way as the air supply, by a measured correlation between flow rate and current absorbed by the electro motor of the pump. Before the electrolyte enters the stacks, its temperature is measured (point f). Then the electrolyte is in parallel divided over the different stacks and cells. After the passage through the fuel cells, the temperature is measured (point g) and the electrolyte is cooled in an external heat exchanger. The hydrogen (99.98% purity) is delivered as pressurized gas to the system at ambient temperature (point a). It runs serially through the stacks. To prevent blockage by water droplets, the direction will be alternated (not shown in drawing). Finally the electric current and cell voltages are measured by the cell voltage monitoring (CVM) (point h) [18]. First every cell is electrically in parallel connected with three neighbouring cells. These groups of four cells are than serially connected in a stack (24 groups or 96 cells in each stack). Finally the (four) stacks are serially connected to each other. An external device will convert the DC-current to AC. To validate the model the average cell and total system values were used. All the described measurements are logged with a time step of one second. Several steady state points were gathered by keeping the current constant and averaging KOH-temperature within acceptable range. The temperature is controlled by a cooler in the secondary circuit, which cools the electrolyte. Not every working point could be reached because the capacity of the cooler was limited. The combination of high currents and low temperature was therefore not possible. Secondly at low currents it was not possible to reach high temperatures as there was no external heater in the electrolyte circuit. Because the goal of this study is to get a model for normal working range, these limitations were acceptable.

Table 2
List of all maximum standard deviations for each dataset.

Parameter	σ_{max}
Total Current	2 A
Total Voltage	2 V
Air Flow Rate	$0.183\,kmol\,h^{-1}$
Air Outlet Temperature	2 °C
Electrolyte Flow Rate	$2.2\,kmol\,h^{-1}$
Electrolyte Temperature Inlet	4 °C
Electrolyte Temperature Outlet	4 °C

3.2. Data analysis

All gathered data – which were obtained during 1 week of experiments – were chronologically obtained and small fluctuations were inevitable. To reduce the amount of data to a workable set of working points, all data were stored and divided in several datasets. The boundary condition to every dataset is that current and temperature are at least 10 s within a certain range (±2.5 ° C and 2.5 A) without interruption. For each dataset, an average value and standard deviation is calculated for each parameter. If the standard deviations for the measured parameters are within the limitations as described in Table 2, the dataset is considered as a valuable working point for model validation. This led to a 50 valuable working points, containing information about electrolyte flow rate, inlet and outlet temperatures, about air flow rate and temperature, about cell current and voltage.

3.3. Discussion on experimental results

Voltage and current: fuel cell performance

To examine the performance of the fuel cell system, all experimental data are shown in a current–voltage diagram or polarization curve (Fig. 4). The horizontal axis shows the total current of the fuel cell system, which is a measure for the current density. The vertical axis shows the total voltage of the fuel cell system. As expected the voltage drops with rising current.

Fuel cell performance and the electrolyte temperature

To examine the influence of the electrolyte temperature the data were divided in three data sets. Each data set represents a number of data points within a certain temperature range of the electrolyte input flow.

- The blue dots represent experimental data with an electrolyte temperature between 25 ° C and 40 °C.
- The red squares represent data at a temperature between 40 ° C and 60 °C.
- The green triangles represent the experiments at relatively high temperature from 60 ° C to 75 °C.

After comparing these three sets of data, can be concluded the voltage is increased with temperature (Fig. 4).

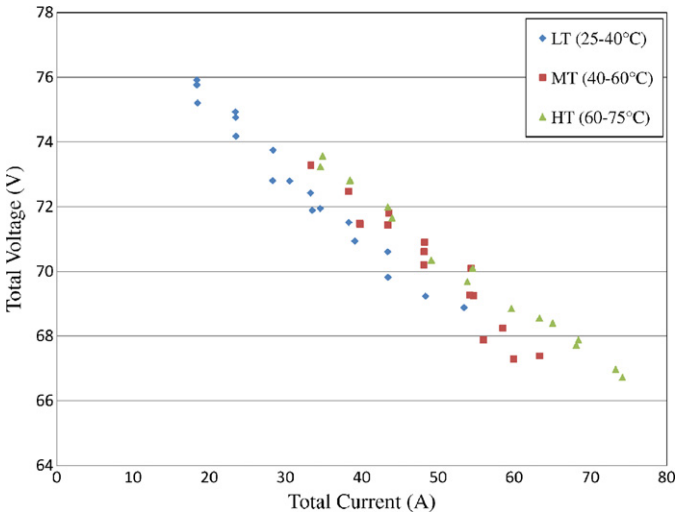

Fig. 4. Polarization curve for different electrolyte temperature ranges (experimental).

Production of useful heat

The electrolyte flow is kept almost constant. The rise in temperature is therefore a good indication of the useful heat production. In Fig. 5 the influence of temperature and electricity load at useful heat production is illustrated. The vertical axis shows the temperature rise of the electrolyte, which is representative for the heat production. The horizontal axis shows the total electricity production (DC) of the fuel cell system. The data points shown on the graph are divided in three groups, according to their temperature range. This is similar to the discussion on the polarization curve.

At high temperature a linear relation between electricity generation and heat production is noticeable. At lower temperature this linear relation is not clear, although it would be expected. At lower temperature the small changes in environment temperature are of a bigger influence than at higher temperature. Comparing high and low temperature the rise in temperature will be higher at low temperature. This is expected because less heat is lost in air flow and losses to the environment.

The air temperature and flow

The air flow rate fluctuates very much and the data points themselves also show a relatively large standard deviation. The air flow is a regulating parameter in the water and temperature control and therefore could not be fixed; a certain fluctuation was inevitable.

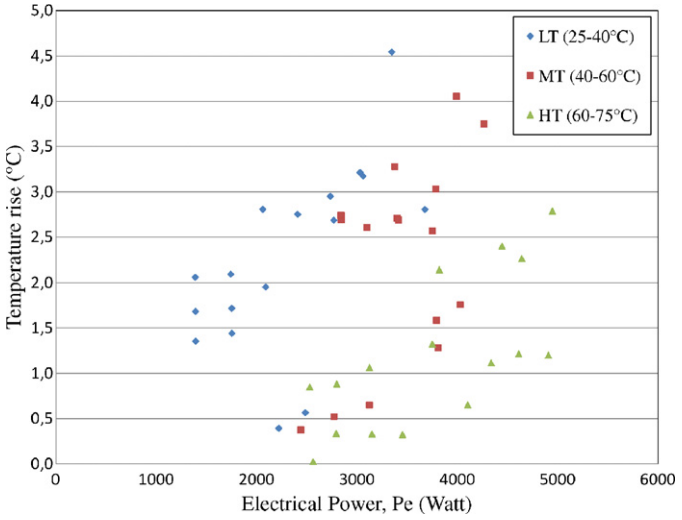

Fig. 5. Useful heat (rise in electrolyte temperature) compared to power output.

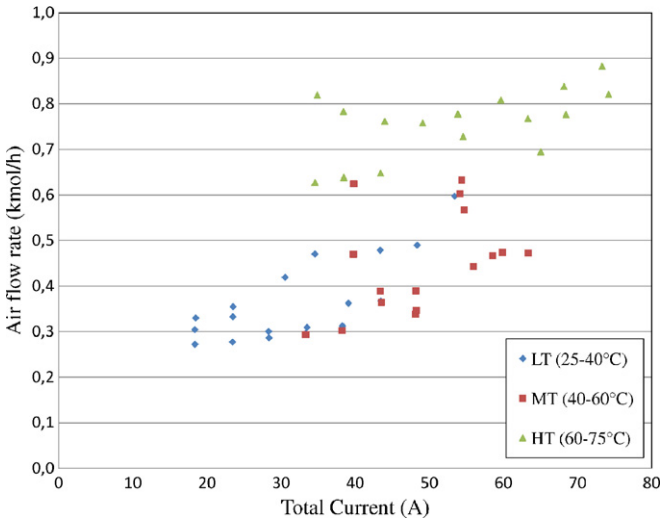

Fig. 6. Air flow in function of electric current at different temperatures.

Comparing air flow rate and total electric current at different electrolyte temperatures, a linear correlation is shown at temperatures below 60 °C, despite the large fluctuations (Fig. 6).

At higher temperature this correlation also exists but the flow rate is increased for better cooling and removal of the water vapour. Above and under 60 °C, the designed working temperature, a different control strategy is used.

As shown in Fig. 7 the air temperature follows the electrolyte temperature. No influence of the different air flow rates for the high temperatures was noticed. (See also next section)

4. Model validation

The model was verified with experiments on stack level. Current, hydrogen input temperature, electrolyte input flow and temperature and air input flow and temperature were input data for our model and experimental set-up (See Section 4) and the model is validated by comparing the fuel cell voltage and output temperatures for both electrolyte and air. A number of modelled and measured data points are shown to illustrate the results in Table 3. The difference between the original and improved model has only got an impact on the air temperature. Only at the discussion of this parameter the models will be compared to each other. First the model is validated at voltage and electrolyte temperature.

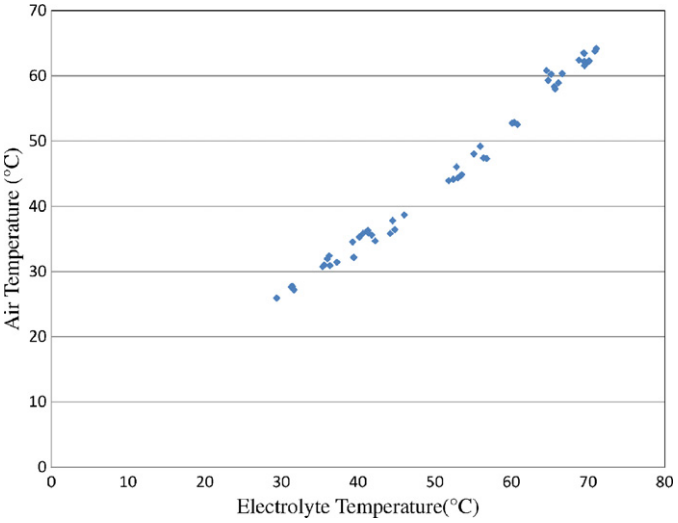

Fig. 7. Relation between air and electrolyte temperature (experimental).

Table 3
Number of modelled and measured data points.

Data Points			Experimental			Model			Improved Model		
nr	I_{stack} A	$T_{in,el}$ °C	U_{stack} V	$T_{el,out}$ °C	$T_{air,out}$ °C	U_{stack} V	$T_{elec,out}$ °C	$T_{air,out}$ °C	U_{stack}	$T_{elec,out}$	$T_{air,out}$
1	18.5	29.4	75	31	28	75	31	30	75	31	28
2	28.3	33.4	73	36	32	73	36	35	73	36	31
3	33.3	37.9	72	41	36	72	40	40	72	40	35
4	39.7	54.0	71	57	47	71	55	51	71	55	48
5	43.4	34.0	70	37	31	70	38	36	70	38	33
6	48.2	53.2	71	56	49	70	55	53	70	55	47
7	53.4	39.4	69	42	35	68	44	38	68	44	39
8	58.5	49.5	68	53	45	68	53	48	68	53	46
9	63.3	49.3	67	53	44	68	54	48	68	54	47
10	74.2	62.9	67	66	58	67	67	51	67	67	62

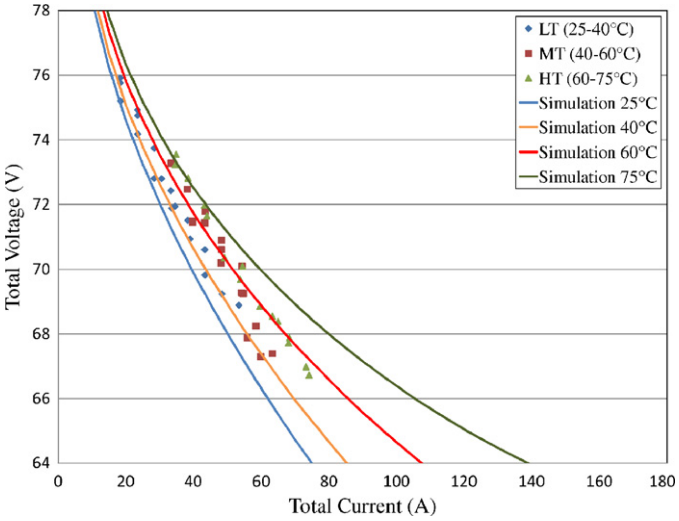

Fig. 8. Polarization curve for different electrolyte temperature ranges (simulation).

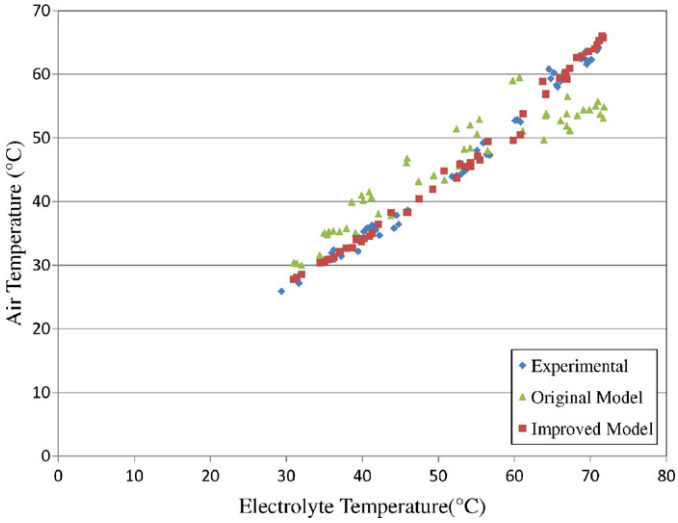

Fig. 9. Relation between air and electrolyte temperature (simulation).

The voltage and the electrolyte temperature

The model shows the same trends for temperature dependency: with a rise in temperature a rise in voltage is achieved. The simulation results, which are presented in Fig. 8 show a good resemblance compared to the experiments.

The air temperature

The linear correlation between electrolyte and air temperature however is not confirmed in the original model (Fig. 9).

At low temperature an overestimation was made and at high temperature (above 60 °C) the model underestimates air temperature. A detailed look at the difference between modelled and measured air temperature shows a linear correlation between model difference and air flow rate (Fig. 10).

Possible explication is the positive effect of the flow rate on convective heat transfer of the air channels and cathode, which was not taken into account in the original model. The improved model uses a correlation (Eq. (18)) between convective heat transfer and velocity. This is based on the definitions of the number of Reynold (Eq. (19)) and Nusselt (Eq. (20)) and the form of their correlation (Eq. (21)). This form is most found in literature (e.g. See References in [19]).

$$Re \sim v \tag{19}$$

$$Nu \sim h_{convection} \tag{20}$$

$$Nu = a.Re^{b} \tag{21}$$

The improved model shows a better result for the prediction of the air temperature (Fig. 9).

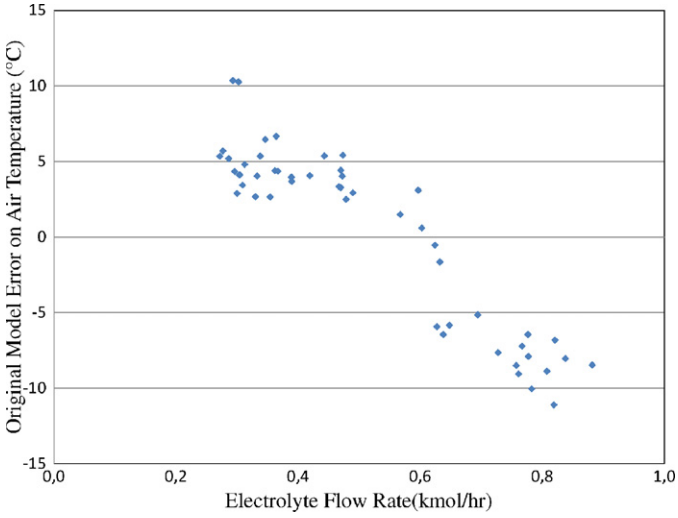

Fig. 10. Simulation error on air temperature prediction in function of air flow rate.

5. Conclusion

The model shows good results in predicting the two most important output parameters, electrolyte temperature and power output, for integrating the AFC into a micro-cogeneration unit. Improvements are made in the prediction of air temperature, which resulted in an acceptable model. The model designed in Aspen Custom

Modeller can now be used to integrate in several energy systems, where an energy and exergy analysis of the system can be performed.

Acknowledgements

The authors would like to thank VITO and KHLim for use of their equipment and are grateful for the advise of Fjo De Ridder, Adwin Martens, Peter Coenen (VITO) and Johan Geenen (Intensys) with the experimental work and data analysis.

References

[1] G.F. Mclean, T. Niet, S. Prince-Richard, N. Djilali, International Journal of Hydrogen Energy 275 (2002) 507–526.
[2] A. Musa, H.-J. Steeman, M. De Paepe, Journal of Fuel Cell Science and Technology 4 (February (1)) (2007) 65–71.
[3] A. Musa, M. De Paepe, International Journal of Hydrogen Energy, 33 (September (17)) (2008) 4665–4672.
[4] A. Musa (Promotor: M. De Paepe), Ph.D.Thesis: Fuel Cell Power Cycles for Future Power Supply, Department of Flow, Heat and Combustion Mechanics, University of Ghent-UGent (2008).
[5] Martin. Pehnt, Environmental Science and Policy II (2008) 25–37.
[6] H.I. Onovwiona, V.I. Ugursal, Renewable and Sustainable Energy Reviews 10 (2006) 389–431.
[7] S. Campanari, E. Macchi, G. Manzolini, International Journal of Hydrogen Energy 33 (2008).
[8] Grietus Mulder, Peter Coenen, Adwin Martens, Jef Spaepen, International Journal of Hydrogen Energy 33 (June (12)) (2008) 3220–3382.
[9] M.C. Kimble, R.E. White, Journal of Electrochemical Society 138 (November (11)) (1991) 3370–3382.
[10] Jang-Ho Jo, Sung-Chul Yi, Journal of Power Sources 84 (1999) 87–106.
[11] Matthias Duerr, Sinclair Gair, Andrew Cruden, Jim McDonald, Journal of Power Sources 171 (September (2)) (2007) 1023–1032.
[12] S. Rowshanzamir, M. Kazemeini, M. Kabiri Isfahani, Journal of Hydrogen Energy 23 (June (6)) (1998) 499–506.
[13] H. Huisseune, Arnout Willockx, Michel De Paepe, International Journal of Hydrogen Energy 33 (November (21)) (2008) 6270–6280.
[14] J. Wu, X.Z. Yuan, H. Wang, M. Blanco, J.J. Martin, J. Zhang, International Journal of Hydrogen Energy 33 (2008) 1735–1746.
[15] Betty Y.S. Lin, Donald W. Kirk, Steven J. Thorpe, Journal of Power Sources 161 (2006) 474–483.
[16] Ryan O'Hayre, Suk-Won Cha, Whitney Colella, Fritz B. Prinz, Fuel Cell Fundamentals, Chapter 6: Fuel Cell Modelling, 2006, pp. 169–192.
[17] J.C. Amphlett, R.F. Mann, B.A. Peppley, P.R. Robergy, A. Rodrigues, Journal of Power Sources 61 (1–2) (1996) 183–188.
[18] G. Mulder, F. De Ridder, P. Coenen, D. Weyen, A. Martens, International Journal of Hydrogen Energy 33 (October (20)) (2008) 5728–5737.
[19] C. Depcik, D. Assanis, A universal heat transfer correlation for intake and exhaust flows in an spark-ignition internal combustion engine, SAE Paper 2002-01-0372.